Physics Letters A 395 (2021) 127229

Contents lists available at ScienceDirect

Physics Letters A

www.elsevier.com/locate/pla

Toward two-dimensional ionic crystals with intrinsic ferromagnetism

Li-Rong Cheng, Zheng-Zhe Lin *

School of Physics and Optoelectronic Engineering, Xidian University, Xi'an 710071, China

ARTICLE INFO

Article history:
Received 29 September 2020
Received in revised form 8 January 2021
Accepted 12 February 2021
Available online 18 February 2021
Communicated by L.M. Woods

Keywords:
2D ferromagnetism
Spin wave
Magnetic anisotropy

ABSTRACT

Modern advanced technologies have been employed to synthesize new two-dimensional (2D) materials of various compositions. Since ionic bonds have no orientation, the ability of 2D ionic crystals to resist thermal fluctuation perpendicular to the 2D surface is worth studying. In this paper, we propose a theoretical analysis on the existence of 2D ionic EuS crystals. Although the Mermin-Wagner theorem denies the possibility of long-range magnetic order in 2D systems, our theoretical model predicts that 2D EuS crystals are ferromagnetic semiconductors. The mechanism of magnetic anisotropy in maintaining the magnetic order is uncovered. The model indicates the effect of the low-energy gap in the spin-wave spectrum on preventing thermal disturbance from destroying the ferromagnetism. A new type of magnetic interaction in 2D EuS crystals is revealed, which leads to the enhancement of Curie temperature by applying a gate voltage. Our theoretical research can benefit future research of other magnetic 2D crystals.

1. Introduction

The development of new two-dimensional (2D) materials promotes improvements in new technologies and devices. 2D compounds may be obtained by mechanical exfoliation from bulks. It is noteworthy that mechanical exfoliation only works for layered crystals where the bulk structures consist of weakly bound layers which can be detached and transferred onto substrates [1,2]. Even so, ionic materials with atomic thickness are still desired. Recently, Na_2Cl and Na_3Cl as 2D Na-Cl crystals are observed on reduced graphene oxide membranes and graphite surface [3]. Decades ago, Landau's theory predicted that the thermal fluctuation in low-dimensional systems is of the same order of magnitude as the size. Since ionic bonds have no orientation, the ability of 2D ionic crystals to resist thermal fluctuation perpendicular to the 2D surface is an important factor related to the existence of free-standing 2D ionic crystals. A recent study reports on the existence of exotic hexagonal NaCl thin films [4] and ionic materials with atomic thickness are proposed to be used as gate dielectrics in field-effect transistors [4,5]. Overall, the exploration of 2D ionic crystals is significant to the current research of materials.

For a long time, people keep seeking spintronics materials using for data storage and manipulation. Several techniques are developed to exploit electron spin for logical operations. Manipulating the electron spin states is a superior route for information processing with lower energy consumption [6]. In spin field-effect transistors, 2D electron gas in the interface of semiconductor heterojunction is employed as a transport layer for spin current. However, 2D electron gas between ferromagnetic (FM) electrodes always suffers from low spin injection efficiency. To solve this problem, people have paid attention to magnetic semiconductors, e.g. EuS [7], (In, Mn)As [8] and (Ga, Mn)As [9,10]. The recent development of 2D materials brings opportunities for finding new spintronic materials. 2D magnetic semiconductors can be ideal materials for transmitting spin current. Nonvolatile control of 2D magnets is proposed as an important technology for magnetoelectric devices [11]. However, the Mermin–Wagner theorem [12] asserts that long-range magnetic order cannot exist in an isotropic 2D system. Fortunately, in recent study [13] people have found 2D layered systems with intrinsic magnetocrystalline anisotropy (e.g. CrI_3 [14–18], $Cr_2Ge_2Te_6$ [19] and $CrSiTe_3$ [20]). The study on 2D magnetic semiconductors will promote the implementation of emerging spintronics devices.

In this paper, theoretical evidence is provided to indicate the existence and stability of 2D ionic EuS crystals. Atomically thin EuS layers are proved to be magnetic semiconductors with the valence and conduction bands consisted of Eu $4f$ and $5d$ orbitals, respectively. A theoretical model is proposed to uncover the mechanism of magnetic anisotropy in maintaining the long-range magnetic order of 2D systems. A new type of magnetic interactions between Eu atoms is revealed. Based on the mechanism, a gate voltage is introduced as an approach to enhance the Curie temperature. The theoretical method used in this work can be extended to future research of 2D magnetic systems.

* Corresponding author.
E-mail address: zzlin@xidian.edu.cn (Z.-Z. Lin).

https://doi.org/10.1016/j.physleta.2021.127229
0375-9601/

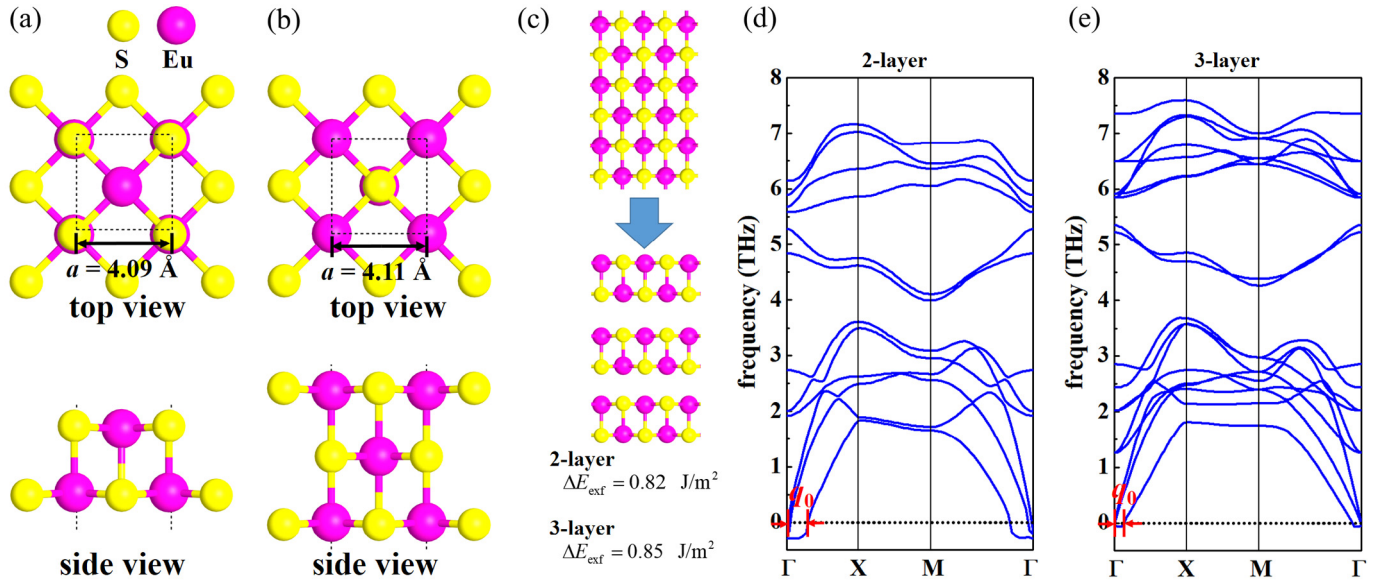

Fig. 1. The structure and stability of 2D EuS. **(a)** The structure of 2-layer EuS. **(b)** The structure of 3-layer EuS. **(c)** The exfoliation of 2D EuS layers from bulk. **(d)** The phonon spectrum of 2-layer EuS. **(e)** The phonon spectrum of 3-layer EuS.

2. Theory

2.1. DFT calculation

To evaluate the structure, thermal stability and electronic properties of 2D ionic EuS crystals, density functional theory (DFT) calculations are performed within the projector augmented-wave method [21,22] as implemented in the Vienna *ab initio* simulation package [23–26]. Plane-wave basis with a kinetic energy cutoff of 400 eV is employed. Convergence is achieved with the energy difference between two successive iteration steps less than 10^{-5} eV. The spin-orbit coupling (SOC) is included in the computation. The Brillouin zone is sampled in $15\times15\times1$ Monkhorst-Pack grid. The correction of van der Waals interactions is treated by the DFT-D3 method with Becke–Jonson damping [27,28].

The primitive cell of 2-layer and 3-layer EuS is exhibited in Fig. 1(a) and Fig. 1(b), respectively, with the periodic boundary shown by dashed lines. Along the direction perpendicular to the 2D EuS surface, a vacuum layer of 12 Å is set up. Geometry relaxations are performed at the level of Perdew-Burke-Ernzerhof (PBE) functional [29] until all the atomic forces are below 0.001 eV/Å. Then, phonon spectra are calculated to verify the stability of the sructures. To obtain reliable results of the energy bands and the projected density of states (PDOS), the hybrid Heyd-Scuseria-Ernzerhof (HSE06) functional [30,31] is employed in the electronic structure calculations. In the computation for evaluating the Heisenberg coupling, the PBE functional plus Hubbard U (PBE+U) is taken with a U value adjusted to reproduce a result of electronic properties that are close to HSE06. The PBE+U method saves computation time, and also provides credible predictions on the magnetic properties.

2.2. Magnon and magnetic order

Mermin and Wagner demonstrated that spin-rotational invariant systems with short range exchange interactions cannot possess long-range magnetic order [12]. Thus, in isotropic 2D systems, the gapless magnon spectrum leads to a divergence of thermal distribution. This indicates that the long-range magnetic order in isotropic 2D systems will be destroyed at finite temperature. But in anisotropic 2D systems, the low-energy gap in magnon spectrum protects the long-range magnetic order escaping from thermal disturbance. To understand the mechanism, let us start from the Heisenberg model. The Heisenberg Hamiltonian in anisotropic 2D systems reads

$$H = -D\sum_i S_{iz}^2 - J\sum_{ij\in \mathrm{NN}} \vec{S}_i \bullet \vec{S}_j . \tag{1}$$

Here, $\vec{S}_i$ denotes the spin of the i^{th} Eu^{2+} ion. J is the Heisenberg coupling between nearest neighbors (NNs) (Fig. 4(a)). D describes the single-ion anisotropy of Eu. $D > 0$ favors off-plane easy axis. Now, the spins in the Hamiltonian (1) should be treated as quantum operators within the linear spin wave approximation (SWA). According to the Holstein–Primakoff representation [32], the spin operators are expressed in terms of bosonic operators

$$S_i^+ = \sqrt{2S}\sqrt{1-\frac{b_i^+ b_i}{2S}}\,b_i \tag{2}$$

$$S_i^- = \sqrt{2S}\,b_i^+\sqrt{1-\frac{b_i^+ b_i}{2S}} \tag{3}$$

$$S_{iz} = S - b_i^+ b_i \tag{4}$$

with b_i and b_i^+ the bosonic annihilation and creation operators on the site (here $S = 7/2$ is the spin of Eu^{2+} ion with $4f^7$ configuration). Such representation leads to a complicated non-linear Hamiltonian. SWA consists of only the quadratic terms in the bosonic operator b. Such approximation is valid for low-energy excitation, i.e. small occupations of the bosonic modes. By SWA, the Hamiltonian (1) reads

$$H_{\mathrm{SWA}} = 2S\sum_i (D + n_i J) b_i^+ b_i - 2JS\sum_{ij\in \mathrm{NN}} b_i^+ b_j \tag{5}$$

where n_i is the numbers of NNs of the i^{th} Eu^{2+} ion. The magnon spectrum can be gotten from the spin wave Hamiltonian (5).

For the square primitive cell of 2-layer EuS with a lattice constant a (Fig. 1(a)) and $n_i = 8$, the Blöch Hamiltonian reads

$$H_{\mathrm{SWA}}(\vec{k}) = \begin{pmatrix} \varepsilon_0 - JSf_{11}(\vec{k}) & -JSf_{12}(\vec{k}) \\ -JSf_{12}(\vec{k}) & \varepsilon_0 - JSf_{11}(\vec{k}) \end{pmatrix} \tag{6}$$

where the on-site energy $\varepsilon_0 = 2S(D + 8J)$, $f_{11}(\vec{k}) = 4(\cos k_x a + \cos k_y a)$ and $f_{12}(\vec{k}) = 4\left(\cos\frac{k_x+k_y}{2}a + \cos\frac{k_x-k_y}{2}a\right)$. The resulting magnon spectrum is

$$E(\vec{k}) = \varepsilon_0 - JSf_{11}(\vec{k}) \pm JS\left|f_{12}(\vec{k})\right|. \tag{7}$$

This spectrum contains a low-energy gap $\Delta = \varepsilon_0 - 16JS = 2SD$.

For the 3-layer EuS (Fig. 1(b)) with $n_1 = 8$, $n_2 = 12$ and $n_3 = 8$, the Blöch Hamiltonian reads

$$H_{\mathrm{SWA}}(\vec{k}) = \begin{pmatrix} \varepsilon_{01} - JSf_{11}(\vec{k}) & -JSf_{12}(\vec{k}) & 0 \\ -JSf_{12}(\vec{k}) & \varepsilon_{02} - JSf_{11}(\vec{k}) & -JSf_{12}(\vec{k}) \\ 0 & -JSf_{12}(\vec{k}) & \varepsilon_{01} - JSf_{11}(\vec{k}) \end{pmatrix} \tag{8}$$

where the on-site energies are $\varepsilon_{01} = 2S(D + 8J)$ and $\varepsilon_{02} = 2S(D + 12J)$. The solutions are

$$E(\vec{k}) = \frac{1}{2}(\varepsilon_{01} + \varepsilon_{02} - 2JSf_{11}(\vec{k}) \pm \sqrt{(\varepsilon_{01} - \varepsilon_{02})^2 + 8J^2S^2f_{12}^2(\vec{k})}) \tag{9}$$

and

$$E(\vec{k}) = \varepsilon_0 - JSf_{11}(\vec{k}). \tag{10}$$

The lowest band also contains a low-energy gap $\Delta = \frac{1}{2}(\varepsilon_{01} + \varepsilon_{02} - 16JS - \sqrt{(\varepsilon_{01} - \varepsilon_{02})^2 + 512J^2S^2}) = 2SD$, which is the same as that of 2-layer EuS.

At zero temperature $T = 0$, all the local magnetic moments are perfectly arranged in a same direction. For $T > 0$, the magnon modes are excited. To estimate the low-energy excitation, the magnon spectrum around the energy minima (i.e. the Γ point) is expanded as $E(\vec{k}) \approx \Delta + \rho k^2$ (for 2-layer $\rho = 3JSa^2$, for 3-layer $\rho = \frac{10}{3}JSa^2$). According to the bosonic statistics, the magnetization of one primitive cell reads

$$M = M_0 - \frac{a^2}{(2\pi)^2}\int_{BZ}\frac{d^2\vec{k}}{e^{E(\vec{k})/k_BT} - 1} \tag{11}$$

where M_0 is the magnetization at $T = 0$ (for 2-layer $M_0 = 2S$, for 3-layer $M_0 = 3S$). In the absence of magnetic anisotropy, $\Delta = 0$ leads to an infinite integral

$$\int_{BZ}\frac{d^2\vec{k}}{e^{E(\vec{k})/k_BT} - 1} \approx k_BT\int_{BZ}\frac{d^2\vec{k}}{\rho k^2} \to \infty. \tag{12}$$

This divergence indicates that 2D long-range magnetic order cannot persist without magnetic anisotropy. The magnetic anisotropy leads to a non-zero gap $\Delta > 0$ and protects the magnetic order at finite temperature.

To estimate the Curie temperature, we now turn to the nonlinear spin wave theory. The initial expressions (2) and (3) are expanded up to

$$S_i^+ \approx \sqrt{2S}(1 - \frac{b_i^+b_i}{4S})b_i \tag{13}$$

$$S_i^- \approx \sqrt{2S}b_i^+(1 - \frac{b_i^+b_i}{4S}). \tag{14}$$

The Hamiltonian (1) containing high-order terms of bosonic operators is not exactly solvable. We deal with the fourth-order term by a substitution

$$\begin{aligned} b_i^+b_ib_j^+b_j &= (<b_i^+b_i> + C_i)(<b_j^+b_j> + C_j) \\ &= <b_i^+b_i><b_j^+b_j> + b_i^+b_i<b_j^+b_j> \\ &\quad - <b_i^+b_i><b_j^+b_j> + C_iC_j \\ &\to <b_i^+b_i><b_j^+b_j> + b_i^+b_i<b_j^+b_j>. \end{aligned} \tag{15}$$

Here C_i is the perturbation terms. The last step removes the constant term and ignores the high-order perturbation. Using a mean-field approximation [33,34], we have

$$\begin{aligned} S_{iz}S_{jz} &= (S - b_i^+b_i)(S - b_j^+b_j) \\ &= S^2 - S(b_i^+b_i + b_j^+b_j) + b_i^+b_ib_j^+b_j \\ &\to -(S - <b^+b>)(b_i^+b_i + b_j^+b_j) \end{aligned} \tag{16}$$

and

$$S_i^+S_j^- \to 2Sb_ib_j^+(1 - \frac{<b^+b>}{S}) \tag{17}$$

$$S_i^-S_j^+ \to 2Sb_i^+b_j(1 - \frac{<b^+b>}{S}). \tag{18}$$

With $M = M_0(S - <b^+b>)/S$, the above results are equivalent to making substitutions $b_i^+b_i \to \frac{M}{M_0}b_i^+b_i$ and $b_i^+b_j \to \frac{M}{M_0}b_i^+b_j$ in H_{SWA}. Such renormalization leads to a self-consistent equation

$$M(T) = M_0 - \frac{a^2}{(2\pi)^2}\int_{BZ}\frac{d^2\vec{k}}{e^{E(\vec{k})M(T)/M_0k_BT} - 1}. \tag{19}$$

This equation implies that the temperature T reduces the energies of magnon quasiparticle and decreases the low-energy gap. At a given temperature T, the magnetization $M(T)$ can then be derived by numerically solving this equation.

2.3. $4f-5d$ indirect exchange

Here we provide a model to describe the magnetic interactions between neighboring Eu^{2+} ions. Eu^{2+} ions have an electronic configuration of $4f^7$ ($S = 7/2$), in which the orbital radius is small. So Eu^{2+} ions are difficult to contact with their neighbors, and the direct exchange should be weak. In magnetic ionic crystals, positive ions usually interact by superexchange which is transmitted by the p electrons of neighboring negative ions. However, DFT calculations show that the conduction bands above Eu $4f$ orbitals are mainly composed by Eu $5d$ orbitals (Fig. 2(a) and (c)), and the S $3p$ orbitals are very high above Eu $4f$ orbitals ($\sim$ 10 eV). So it is very difficult to realize the $4f$-$3p$-$4f$ superexchange. We infer that the magnetic interactions are intermediated by a mechanism of $4f$-$5d$ indirection exchange, which is exhibited in the following text.

For two ideal Eu^{2+} ions A and B, the atomic orbitals are $4f$ (half-filled) and $5d$ (empty). The Hamiltonian reads

$$\begin{aligned} H_0 &= \varepsilon_{4f}\sum_{i\in A4f}a_i^+(\sigma_A)a_i(\sigma_A) + \varepsilon_{5d}\sum_{i\in A5d}a_i^+(\sigma_A)a_i(\sigma_A) \\ &\quad + \varepsilon_{4f}\sum_{i\in B4f}a_i^+(\sigma_B)a_i(\sigma_B) + \varepsilon_{5d}\sum_{i\in B5d}a_i^+(\sigma_B)a_i(\sigma_B) \end{aligned} \tag{20}$$

Here, σ_A / σ_B denotes the spin direction in ion A / B. a_i is the fermionic operator on the orbital i. The hexahedral crystal field of neighboring S^{2-} may influent the electrons in Eu^{2+}. This effect reads

$$\begin{aligned} H_c' &= \sum_{\substack{i\in A4f \\ j\in A5d}}t_{ij}\left(a_j^+(\sigma_A)a_i(\sigma_A) + a_i^+(\sigma_A)a_j(\sigma_A)\right) \\ &\quad + \sum_{\substack{i\in B4f \\ j\in B5d}}t_{ij}\left(a_j^+(\sigma_B)a_i(\sigma_B) + a_i^+(\sigma_B)a_j(\sigma_B)\right) \end{aligned} \tag{21}$$

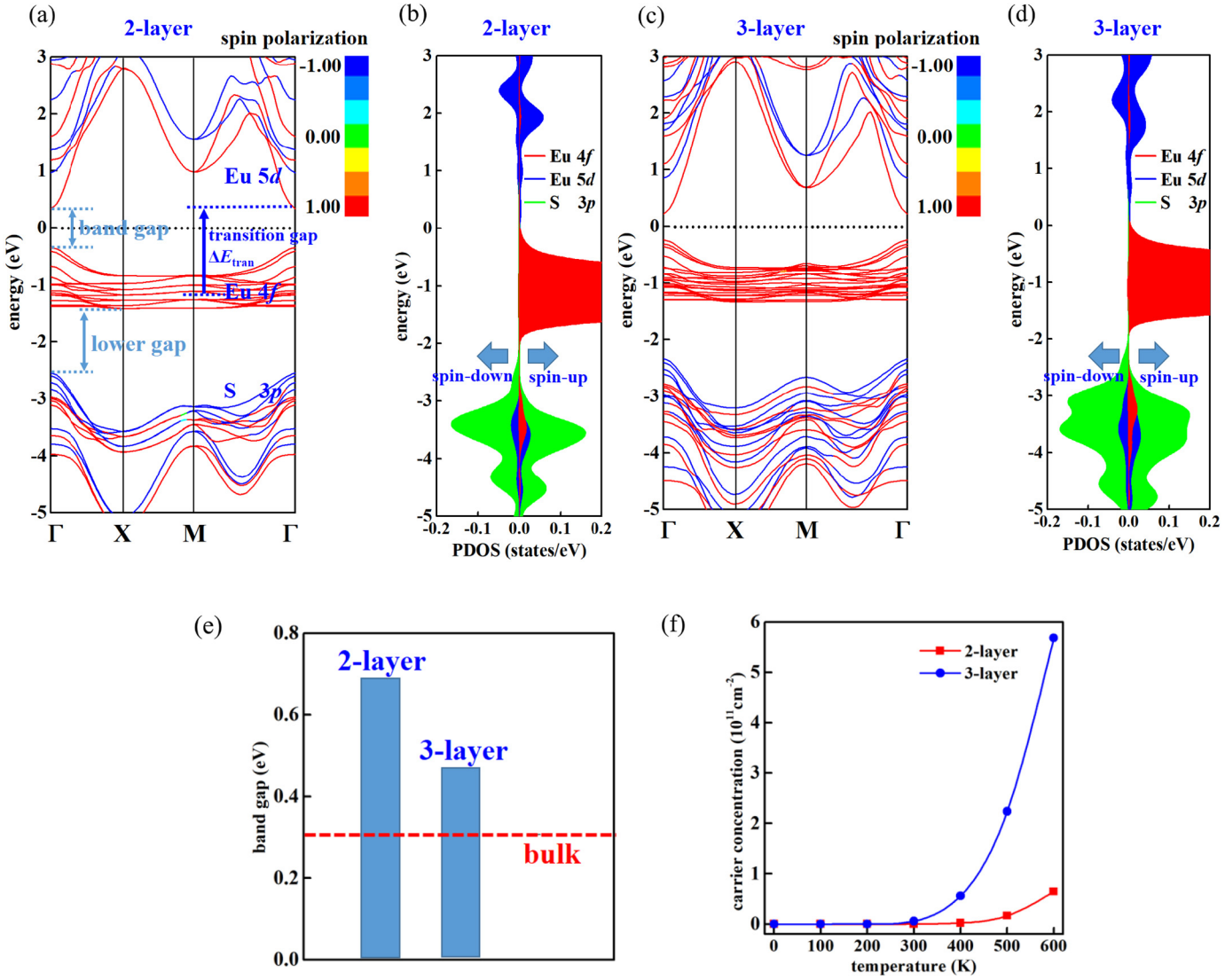

Fig. 2. The electronic structure and properties of 2D EuS. **(a)** The energy bands of 2-layer EuS. **(b)** The PDOS of 2-layer EuS. **(c)** The energy bands of 3-layer EuS. **(d)** The PDOS of 3-layer EuS. **(e)** The band gaps of 2D EuS. **(f)** The carrier concentration in 2D EuS.

where t_{ij} is the hopping. H_c' leads to $4f \rightarrow 5d$ transitions, and the interaction between the excited electrons reads

$$H_{ee}' = \sum V_{i_2 j_2 j_1 i_1} a_{i_2}^{+}(\sigma_A) a_{j_2}^{+}(\sigma_B) a_{j_1}(\sigma_B) a_{i_1}(\sigma_A). \tag{22}$$

We have a total perturbation $H' = H_c' + H_{ee}'$.

The system has a FM ground state $\left|\Psi_g^{FM}\right\rangle = \prod_{i\in A4f} |i(\uparrow)\rangle \times \prod_{j\in B4f} |j(\uparrow)\rangle$ in which the ions A and B are both spin-up. There also exists an antiferromagnetic (AFM) state $\left|\Psi_g^{AFM}\right\rangle = \prod_{i\in A4f} |i(\uparrow)\rangle \prod_{j\in B4f} |j(\downarrow)\rangle$, in which the ion A (B) is spin-up (spin-down). The energy difference between FM and AFM states can be estimated by the perturbation theory. The first-order perturbation energy is $\Delta E^{(1)} = \langle\Psi_g| H' |\Psi_g\rangle = 0$ because H_c' converts the ground state into an excited state that is orthogonal to $|\Psi_g\rangle$ and H_{ee}' does not work on $|\Psi_g\rangle$. The second-order perturbation is

$$\Delta E^{(2)} = \sum_{m\neq g} \frac{\left|\langle\Psi_g| H' |\Psi_m\rangle\right|^2}{E_g - E_m} = \sum_{m\neq g} \frac{\left|\langle\Psi_g| H_c' |\Psi_m\rangle\right|^2}{E_g - E_m}. \tag{23}$$

Here, all the $|\Psi_m\rangle$ are the excited states of the system. For the case of FM and AFM, their $\Delta E^{(2)}$ are the same because H_c' does not contain the spin direction. So, the energy difference of FM and AFM states cannot be distinguished at the level of second-order perturbation. The third-order perturbation reads

$$\begin{aligned}\Delta E^{(3)} &= \sum_{\substack{m\neq g\\ n\neq g}} \frac{\langle\Psi_g| H' |\Psi_m\rangle\langle\Psi_m| H' |\Psi_n\rangle\langle\Psi_n| H' |\Psi_g\rangle}{(E_g - E_m)(E_g - E_n)} \\ &\quad - \Delta E^{(1)} \sum_{m\neq g} \frac{\left|\langle\Psi_g| H' |\Psi_m\rangle\right|^2}{E_g - E_m} \\ &= \sum_{\substack{m\neq g\\ n\neq g}} \frac{\langle\Psi_g| H_c' |\Psi_m\rangle\langle\Psi_m| H' |\Psi_n\rangle\langle\Psi_n| H_c' |\Psi_g\rangle}{(E_g - E_m)(E_g - E_n)}\end{aligned} \tag{24}$$

Since $\langle\Psi_g| H_c' |\Psi_m\rangle$ involves only single excitation to $5d$, we have

$$\Delta E^{(3)} = \frac{\sum_{\substack{m\neq g\\ n\neq g}} \langle\Psi_g| H_c' |\Psi_m\rangle\langle\Psi_m| H' |\Psi_n\rangle\langle\Psi_n| H_c' |\Psi_g\rangle}{(\varepsilon_{5d} - \varepsilon_{4f})^2}. \tag{25}$$

In $\langle\Psi_m| H' |\Psi_n\rangle = \langle\Psi_m| H_c' |\Psi_n\rangle + \langle\Psi_m| H_{ee}' |\Psi_n\rangle$, only H_{ee}' contributes to the energy difference $\Delta E_{FM}^{(3)} - \Delta E_{AFM}^{(3)}$ and the main con-

tributions are m = n. For the FM state, the terms $\langle \Psi_m | H'_{ee} | \Psi_m \rangle$ involve both Coulomb repulsion and exchange. However, for the AFM state, the terms $\langle \Psi_m | H'_{ee} | \Psi_m \rangle$ only involve Coulomb repulsion because the spin directions σ_A and σ_B in H'_{ee} are opposite. Finally, we can approximately estimate that

$$\Delta E^{(3)}_{FM} - \Delta E^{(3)}_{AFM} \propto \frac{1}{(\varepsilon_{5d} - \varepsilon_{4f})^2}. \tag{26}$$

3. Results and discussion

2D EuS lattices (Fig. 1(a) and (b)) have tetragonal symmetry with Eu^{2+} and S^{2-} arranging in NaCl type. The lattice constant of 2-layer (3-layer) EuS is a = 4.09 Å (4.11 Å), respectively. The lattices have a very slight compression in the direction perpendicular to the 2D surface (~ 2% of the thickness). The distances of a Eu^{2+} ion to its nearest neighbors are almost the same. For a 2D layered material, the exfoliation energy is important to decide whether it can be peeled off from the bulk. Exfoliation progress is described in Fig. 1(c). The calculated exfoliation energy is ΔE_{exf} = 0.82 (0.85) J/m^2 for 2-layer (3-layer) EuS, which is larger than the two times of graphene (~0.36 J/m^2). Indeed, the exfoliation of ionic crystals is more difficult than layered van der Waals crystals. But the ΔE_{exf} of 2D EuS indicates that it is still possible to be produced from the bulk.

Ionic crystals are held together by electrostatic interactions. The total energy of an N-atom lattice can be expressed as $E = N(-\frac{\alpha q^2}{4\pi\varepsilon_0 r} + \frac{mB}{r^n})$. Here, α = 1.748 is the Madelung constant of EuS bulk, r is the Eu-S bond length and m = 6 is the number of nearest neighbors in EuS bulk. The balanced bond length (i.e. $\partial E/\partial r = 0$) is $r_0 = (\frac{4\pi\varepsilon_0 nmB}{\alpha q^2})^{\frac{1}{n-1}}$. By fitting the total energy from bulk calculations with different r (Supplementary Sec. 1), we get n = 6.36. For 2-layer EuS, the Madelung constant is α = 1.682, and the neighbor number is m = 5. In 2D EuS layers, the reduction of neighbors m leads to a decrease of repulsion energy. But the decrease of Madelung energy is not that much as the repulsion energy. Since $r_0 \propto (m/\alpha)^{\frac{1}{n-1}}$, we can estimate that the bond length in 2-layer EuS is about 2.6% shorter than the bulk. This prediction is coincidence with the previous DFT calculation and reveals the ionic feature of 2D EuS layers.

To verify the dynamic stability of 2D EuS, the phonon spectrum (Fig. 1(d) and (e)) are plotted. We can see a small band of imaginary frequencies near the Γ point. This indicates that free-standing 2D EuS layers have a limit of size, and larger areas become unstable. Such a feature also exists in 2D germanene [35]. We can estimate the size limit of free-standing 2D EuS by the range of imaginary phonon momentum, i.e. 0 ~ q_0. The wavelength of a phonon mode is $\lambda = 2\pi/q$. When the size is smaller than $2\pi/q_0$, the imaginary modes do not work and then free-standing 2D EuS can exist. For 2-layer (3-layer) EuS, the calculated size limit is 27 (57) Å, respectively. So, free-standing 2D EuS can exist in nanoscale.

In the theoretical model in Sec. 2.2, the magnetic anisotropy D is important to decide the thermal stability of long-range magnetic order. Thus, the magnetic anisotropy energy (MAE) is calculated to evaluate D. With tetragonal symmetry, the MAE of 2D EuS exhibits uniaxial anisotropy and can be fit to [36]

$$\text{MAE} = K_1 \sin^2\theta + K_2 \sin^4\theta \tag{27}$$

where θ is the angle relative to the easy axis. By fitting DFT calculation results (Fig. 4(f) and (i)), we have K_1 = -0.24 meV/cell, K_2 = 0 for 2-layer EuS, and K_1 = -0.19 meV/cell, K_2 = 0.04 meV/cell for 3-layer EuS. The maximum MAE, which is defined as the energy difference of the system with magnetization axis along the easy axis and perpendicular to it, is calculated to be 0.24 meV/cell for 2-layer EuS, and 0.15 meV/cell for 3-layer EuS. By $\text{MAE}_{max} = nDS^2$ (n is the number of Eu ions in one primitive cell) the magnetic anisotropy D is finally obtained.

To investigate the electronic properties, the energy bands and PDOS of 2D EuS are plotted. With the SOC, an electron in a certain state does not have a definite spin. The electronic wavefunction is presented as $\Psi = (\Psi_\uparrow(\mathbf{r}), \Psi_\downarrow(\mathbf{r}))^T$, and the spin polarization of a state reads

$$P = \frac{\int |\Psi_\uparrow(\mathbf{r})|^2 d\mathbf{r} - \int |\Psi_\downarrow(\mathbf{r})|^2 d\mathbf{r}}{\int |\Psi_\uparrow(\mathbf{r})|^2 d\mathbf{r} + \int |\Psi_\downarrow(\mathbf{r})|^2 d\mathbf{r}}. \tag{28}$$

We plot each band state with color to show the polarization. For 2-layer EuS, the energy bands and PDOS are plotted in Fig. 2(a) and (b). The S 3p bands lie far below the Fermi level, which constitute the electron orbitals around the S^{2-} ions. The valence bands are composed of Eu 4f orbitals and they are fully spin-polarized. Eu^{2+} ions have a half-filled $4f^7$ configuration. In the rare-earth ions, it should be the most stable. The conduction bands are composed of Eu 5d orbitals. The spin-up bands have lower energy. This electronic structure shows a feature of a magnetic semiconductor with the valence bands top and the conduction bands bottom in the same spin direction. The energy bands and PDOS of 3-layer EuS are plotted in Fig. 2(c) and (d). A similar feature of magnetic semiconductor can be seen. With the quantum confinement effect, the band gaps of 2D EuS layers are larger than EuS bulk (Fig. 2(e)). It is worth noting that 2D EuS layers have a direct band gap, while the band gap of EuS bulk is indirect (for the bands of EuS bulk, please see Supplementary Fig. S1). The carrier concentration of 2D EuS (Fig. 2(f)) can be evaluated by $c = c_n + c_p$. Here, the electron concentration reads $c_n = \int \frac{D(E)dE}{e^{(E-E_F)/k_BT}+1}$ ($D(E)$ is the density of states) and the hole concentration reads $c_p = \int D(E)(1 - \frac{1}{e^{(E-E_F)/k_BT}+1})dE$. The results show that the carrier concentration sharply increases (~ 10^{11} cm^{-2}) at T > 300 K, which is lower than graphene (~ 10^{12} cm^{-2}) by an order of magnitude.

To save computation in the following study, we turn to the PBE+U method and try to find a proper U value to approximate the HSE06 functional. It is known that the PBE functional always underestimates the band gap. Here we consider the band gap and the lower gap (the gap from S 3p band top to the valence band bottom, see Fig. 2(a)). We try a wide range of U values and compare the band gap and the lower gap with those of HSE06 (Fig. 3(a)). However, the two cannot be both matched because the Hubbard U only considers the electron correlation in the narrow Eu 4f bands. The most appropriate value is U = 5 eV, for which the band gap is around the value of HSE06 and the lower gap is not too small. A comparison of bands is shown in Supplementary Fig. S2. We can see that by PBE+U the shapes of valence and conduction bands are roughly close to that of HSE06, while the S 3p bands are a bit higher. Our choice of U is a compromised adaption between the band gap and the lower gap. In the following text, we adopt this U value for the subsequent calculations.

To prove the mechanism of 4f-5d indirect exchange, we turn to Eq. (26) which is the result of three-order perturbation. In the crystal field of S^{2-}, some of the 4f orbitals are affected and some are not due to the symmetry matching. So the 4f flat bands can be seen as unperturbed energy. We estimate $\varepsilon_{5d} - \varepsilon_{4f} = \Delta E_{tran}$ as the gap from the average value of 4f flat bands to the 5d band bottom. To probe the energy difference $E_{AFM} - E_{FM}$ between the FM and AFM states of two neighboring Eu^{2+} ions, we consider the two configurations for 2-layer EuS in Fig. 4(b). By changing the Hubbard U, the electron correlation and $E_{AFM} - E_{FM}$ is then changed. The calculation results (Fig. 3(b)) fit the three-order perturbation theory (Eq. (26)) well.

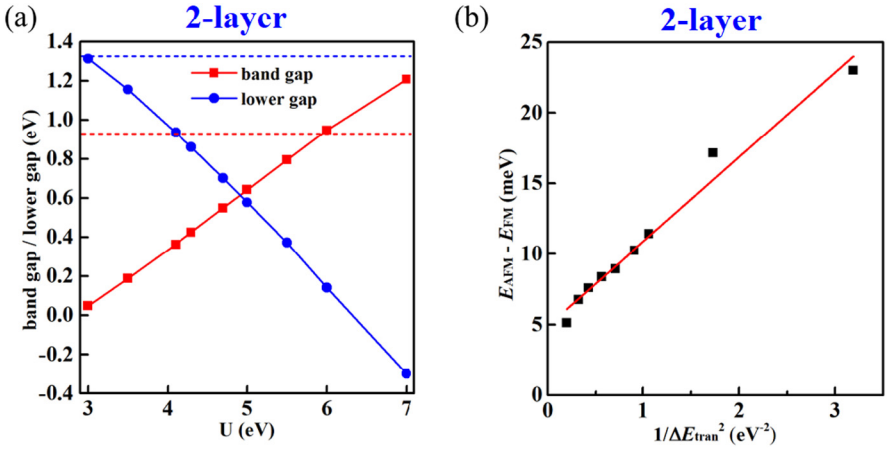

Fig. 3. The electron interactions in 2D EuS. **(a)** The band gap and lower gap of 2-layer EuS at the level of PBE+U. The blue (red) dashed line denotes the band (lower) gap at the level of HSE06. **(b)** The energy difference E_{AFM} - E_{FM} of 2-layer EuS varying with ΔE_{tran}. (For interpretation of the colors in the figure(s), the reader is referred to the web version of this article.)

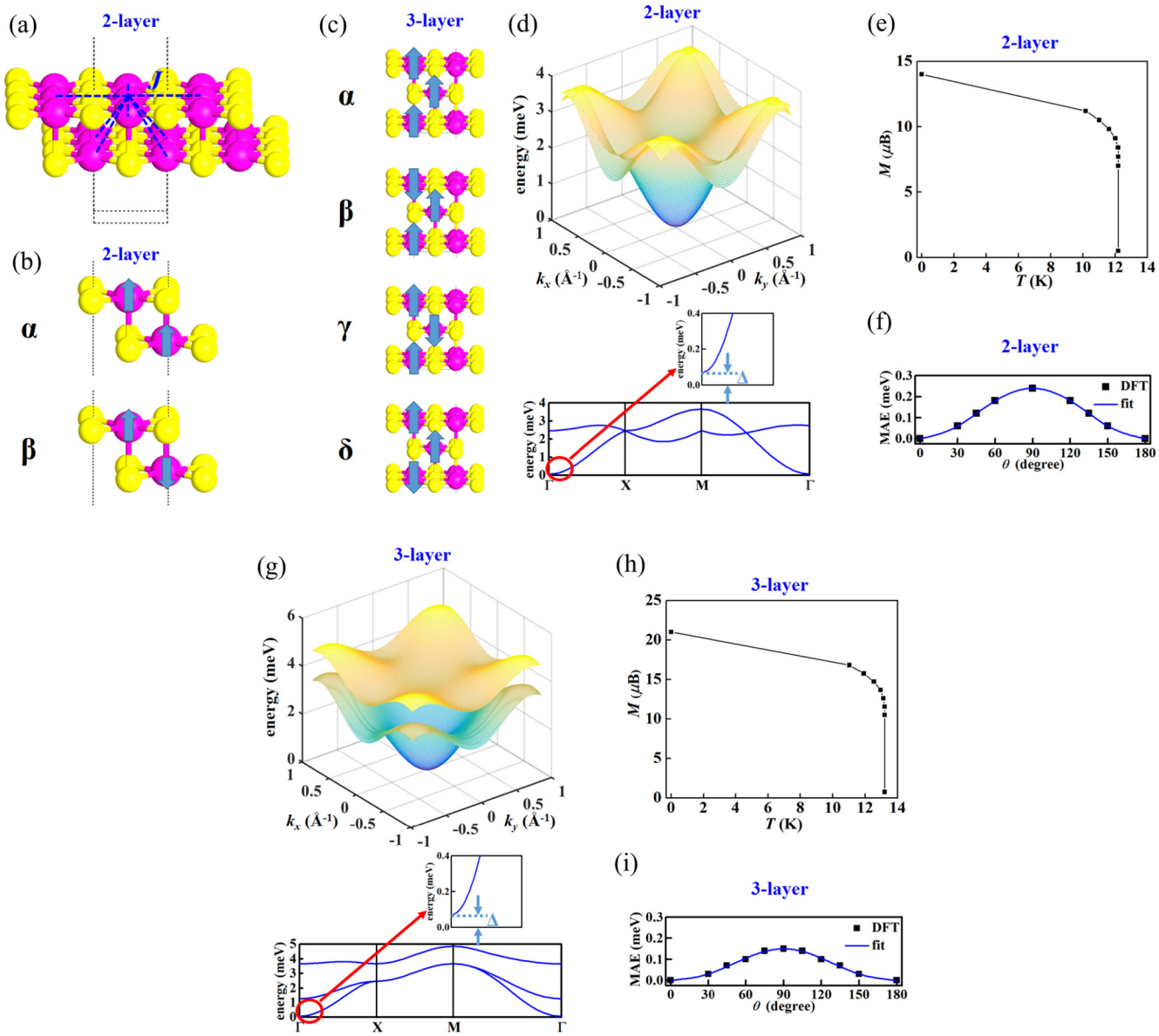

Fig. 4. The magnetic interactions and spin wave in 2D EuS. **(a)** The Heisenberg coupling J in 2D EuS. **(b)** The magnetic configurations of 2-layer EuS. **(c)** The magnetic configurations of 2-layer EuS. **(d)** The magnon spectrum of 2-layer EuS. **(e)** The magnetic moment of 2-layer EuS varying with temperature T. **(f)** MAE of 2-layer EuS. **(g)** The magnon spectrum of 3-layer EuS. **(h)** The magnetic moment of 3-layer EuS varying with temperature T. **(i)** MAE of 3-layer EuS.

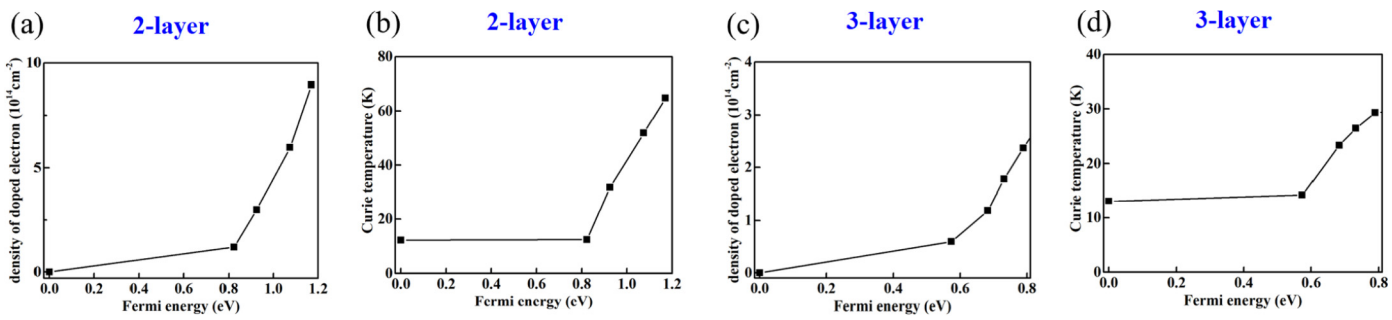

Fig. 5. The effect of gating on 2D EuS. **(a)** The electron density in 2-layer EuS. **(b)** The Curie temperature of 2-layer EuS. **(c)** The electron density in 3-layer EuS. **(d)** The Curie temperature of 4-layer EuS.

Next, to obtain the magnon spectrum, the coupling J between neighboring Eu^{2+} ions (Fig. 4(a)) should be evaluated to map into the Heisenberg model. For 2-layer EuS, every Eu^{2+} ion has four neighbors in one layer and four in the other layer. For the two configurations $\boldsymbol{\alpha}$ and $\boldsymbol{\beta}$ in Fig. 4(b), the Heisenberg energies in one primitive cell are $E_{\boldsymbol{\alpha}} = E_0 - 16JS^2$ and $E_{\boldsymbol{\beta}} = E_0$ (i.e. $E_{\boldsymbol{\beta}} - E_{\boldsymbol{\alpha}} = 16JS^2$). By calculating the energy difference between $\boldsymbol{\alpha}$ and $\boldsymbol{\beta}$, we obtain J = 4.28×10^{-2} meV for the 2-layer EuS. By a similar method, we consider the configurations $\boldsymbol{\alpha}$, $\boldsymbol{\beta}$, $\boldsymbol{\gamma}$ and $\boldsymbol{\delta}$ in Fig. 4(c). The corresponding energies are $E_{\boldsymbol{\alpha}} = E_0 - 28JS^2$, $E_{\boldsymbol{\beta}} = E_0 - 12JS^2$, $E_{\boldsymbol{\gamma}} = E_0 + 4JS^2$ and $E_{\boldsymbol{\delta}} = E_{\boldsymbol{\beta}}$. DFT calculations result in J = 4.52×10^{-2} meV for the 3-layer EuS.

The magnon spectrum of 2-layer (3-layer) EuS is shown in Fig. 4(d) (Fig. 4(g)), respectively. In the lowest band, we can see the low-energy gap Δ = $2SD$ at the Γ point. The magnetization at any temperature T can then be estimated numerically by the self-consistent equation (19). The results (Fig. 4(e) and (h)) shows that the magnetic moment sharply decreases when T is near the Curie temperature. The Curie temperature of 2-layer (3-layer) EuS is about T_c = 12 (13) K, respectively, which is close to the recently discovered 2D ferromagnet Fe_3GeTe_2 [37]. To verify this result, we further perform quantum Monte Carlo simulations for 20 × 20 EuS supercells (for the detail, see Supplementary Sec. 3), and obtain similar M-T curves to Fig. 4(e) and (h).

According to the mechanism of $4f$-$5d$ indirect exchange, the electrons entering the Eu $5d$ orbitals are pivotal to generate the FM interaction. If modulation is employed to let more electrons going into the Eu $5d$ orbitals, the Heisenberg coupling J may be enlarged and the Curie temperature is then enhanced. In experiments, this can be done by applying a gate voltage on 2D EuS. In DFT calculations, it is simulated by enhancing the Fermi level. We calculate the Heisenberg J under given Fermi level by the above method and then obtain the Curie temperature by solving the self-consistent equation (19). The results are shown in Fig. 5. For both 2-layer and 3-layer EuS, the density of free electron increases with enhancing Fermi level. When the Fermi level is elevated up into the Eu $5d$ conduction bands, the electron density and the Curie temperature sharply increases. This result further confirms the theory of $4f$-$5d$ indirect exchange and reveals a pathway to modulate the magnetic properties in 2D magnets.

Finally, we concern about the influence of phonons on the magnon spectrum. In 2D systems, the low-energy gap Δ is important to keep the long-range magnetic order. It is known that magnon-phonon scattering may soften the quasiparticle energies of magnons and then lower Δ. Here, we estimate the effect of longitudinal acoustic (LA) phonons which leads to the stretching of lattice and the change of Heisenberg coupling J. The effective magnon-phonon interaction Hamiltonian is accounted as

$$H_{m-p} \approx S|\nabla J| \sum_{NN,\vec{q},\vec{k}} \sqrt{\frac{\hbar}{2\sigma A\omega(\vec{q})}} 2i|\vec{q}\bullet\vec{R}_{NN}| \times (1-\cos\vec{k}\bullet\vec{R}_{NN})(a^{+}_{\vec{q}}b^{+}_{\vec{k}+\vec{q}}b_{\vec{k}} - a^{+}_{\vec{q}}b^{+}_{\vec{k}-\vec{q}}b_{\vec{k}}). \tag{29}$$

This Hamiltonian $H_{m\text{-}p}$ represents a magnon who releases a virtual phonon and then adsorbs it. At the level of second-order perturbation, the self-energy correction of magnons reads

$$E^{(2)}_{m-p}(\vec{k}) > -\frac{2n\hbar S^2|\nabla J|^2}{\sigma c(\hbar c - 2\rho k)}. \tag{30}$$

The detailed explanation of above theory is presented in Supplementary Sec. 4. For 2- and 3-layer EuS, we finally obtain a rough estimation of $E^{(2)}_{m-p}$> -8×10^{-4} meV. Such small value ensures that the low-energy gap of magnon is protected from the thermal disturbance of phonons.

4. Conclusions

By a combination of the theoretical model and DFT calculations, we systematically provide theoretical pieces of evidence for the existence and stability of 2D ionic EuS layered crystals. 2D magnets with magnetic anisotropy are able to hold long-range magnetic order at finite temperature. Our theoretical model reveals a mechanism beyond the Mermin–Wagner theorem. The model reveals the effect of a low-energy gap in the magnon spectrum on preventing thermal disturbance from destroying the ferromagnetism. 2D EuS layers are proved to be magnetic semiconductors with the valence and conduction bands fully spin-polarized. The mechanism of $4f$-$5d$ indirect exchange between Eu^{2+} ions is uncovered. Our theory clarifies the way of this new type of magnetic interactions, in which the dynamic interactions between the excited Eu $5d$ electrons play an important role in generating the exchange. Based on the mechanism, a gate voltage is introduced as an approach to enhance the Curie temperature. Our theoretical research would benefit future research of other magnetic 2D crystals.

CRediT authorship contribution statement

Li-Rong Cheng: Investigation, Analyzing, Calculation, Writing Original draft preparation. **Zheng-Zhe Lin:** Supervision, Conceptualization, Methodology, Writing Reviewing.

Declaration of competing interest

The authors declare that they have no known competing financial interests or personal relationships that could have appeared to influence the work reported in this paper.

Acknowledgements

This work is supported by the Natural Science Basic Research Plan in Shaanxi Province of China (No. 2018JQ1034).

Appendix A. Supplementary material

Supplementary material related to this article can be found online at https://doi.org/10.1016/j.physleta.2021.127229.

References

[1] K.S. Novoselov, A.K. Geim, S.V. Morozov, D. Jiang, Y. Zhang, S.V. Dubonos, et al., Electric field effect in atomically thin carbon films, Science 306 (2004) 666.
[2] L. Gao, J.R. Guest, N.P. Guisinger, Epitaxial graphene on Cu(111), Nano Lett. 10 (2010) 3512.
[3] G. Shi, L. Chen, Y. Yang, D. Li, Z. Qian, S. Liang, et al., Two-dimensional Na–Cl crystals of unconventional stoichiometries on graphene surface from dilute solution at ambient conditions, Nat. Chem. 10 (2018) 776.
[4] K.A. Tikhomirova, C. Tantardini, E.V. Sukhanova, Z.I. Popov, S.A. Evlashin, M.A. Tarkhov, et al., Exotic two-dimensional structure: the first case of hexagonal NaCl, J. Phys. Chem. Lett. 11 (2020) 3821.
[5] B. Luo, Y. Yao, E. Tian, H. Song, X. Wang, G. Li, et al., Graphene-like monolayer monoxides and monochlorides, Proc. Natl. Acad. Sci. USA 116 (2019) 17213.
[6] S.A. Wolf, D.D. Awschalom, R.A. Buhrman, J.M. Daughton, S. von Molnár, M.L. Roukes, et al., Spintronics: a spin-based electronics vision for the future, Science 294 (2001) 1488–1495.
[7] S. von Molnar, S. Methfessel, Resistivity anomaly in conducting europium chalcogenides, J. Appl. Phys. 39 (1968) 899.
[8] H. Munekata, H. Ohno, S. von Molnár, A. Segmüller, L.L. Chang, L. Esaki, Diluted magnetic III-V semiconductors, Phys. Rev. Lett. 63 (1989) 1849–1852.
[9] H. Ohno, A. Shen, F. Matsukura, A. Oiwa, A. Endo, S. Katsumoto, et al., (Ga, Mn)As: a new diluted magnetic semiconductor based on GaAs, Appl. Phys. Lett. 69 (1996) 363–365.
[10] L. Chen, X. Yang, F. Yang, J. Zhao, J. Misuraca, P. Xiong, S. von Molnár, Enhancing the Curie temperature of ferromagnetic semiconductor (Ga, Mn)As to 200 K via nanostructure engineering, Nano Lett. 11 (2011) 2584–2589.
[11] Y. Zhao, J.-J. Zhang, S. Yuan, Z. Chen, Nonvolatile electrical control and heterointerface-induced half-metallicity of 2D ferromagnets, Adv. Funct. Mater. 29 (2019) 1901420.
[12] N.D. Mermin, H. Wagner, Absence of ferromagnetism or antiferromagnetism in one- or two-dimensional isotropic Heisenberg models, Phys. Rev. Lett. 17 (1966) 1133.
[13] K.S. Burch, D. Mandrus, J.-G. Park, Magnetism in two-dimensional van der Waals materials, Nature 563 (2018) 47.
[14] P. Jiang, C. Wang, D. Chen, Z. Zhong, Z. Yuan, Z.-Y. Lu, et al., Stacking tunable interlayer magnetism in bilayer CrI_3, Phys. Rev. B 99 (2019) 144401.
[15] H.H. Kim, B. Yang, T. Patel, F. Sfigakis, C. Li, S. Tian, et al., One million percent tunnel magnetoresistance in a magnetic van der Waals heterostructure, Nano Lett. 18 (2018) 4885.
[16] T. Song, X. Cai, M.W.-Y. Tu, X. Zhang, B. Huang, N.P. Wilson, et al., Giant tunneling magnetoresistance in spin-filter van der Waals heterostructures, Science 360 (2018) 1214.
[17] Z. Wang, I. Gutierrez-Lezama, N. Ubrig, M. Kroner, M. Gibertini, T. Taniguchi, et al., Very large tunneling magnetoresistance in layered magnetic semiconductor CrI_3, Nat. Commun. 9 (2018) 2516.
[18] N. Sivadas, S. Okamoto, X. Xu, C.J. Fennie, D. Xiao, Stacking-dependent magnetism in bilayer CrI_3, Nano Lett. 18 (2018) 7658.
[19] C. Gong, L. Li, Z. Li, H. Ji, A. Stern, Y. Xia, et al., Discovery of intrinsic ferromagnetism in two-dimensional van der Waals crystals, Nature 546 (2017) 265.
[20] J. Zhang, X. Cai, W. Xia, A. Liang, J. Huang, C. Wang, et al., Unveiling electronic correlation and the ferromagnetic superexchange mechanism in the van der Waals crystal $CrSiTe_3$, Phys. Rev. Lett. 123 (2019) 047203.
[21] G. Kresse, D. Joubert, From ultrasoft pseudopotentials to the projector augmented-wave method, Phys. Rev. B 59 (1999) 1758.
[22] P.E. Blöchl, Projector augmented-wave method, Phys. Rev. B 50 (1994) 17953.
[23] G. Kresse, J. Furthmüller, Efficient iterative schemes for ab initio total-energy calculations using a plane-wave basis set, Phys. Rev. B 54 (1996) 11169.
[24] G. Kresse, J. Furthmüller, Efficiency of ab-initio total energy calculations for metals and semiconductors using a plane-wave basis set, Comput. Mater. Sci. 6 (1996) 15.
[25] G. Kresse, J. Hafner, Ab initio molecular dynamics for liquid metals, Phys. Rev. B 47 (1993) 558.
[26] G. Kresse, J. Hafner, Ab initio molecular-dynamics simulation of the liquid-metal–amorphous-semiconductor transition in germanium, Phys. Rev. B 49 (1994) 14251.
[27] S. Grimme, J. Antony, S. Ehrlich, H. Krieg, A consistent and accurate ab initio parametrization of density functional dispersion correction (DFT-D) for the 94 elements H-Pu, J. Chem. Phys. 132 (2010) 154104.
[28] S. Grimme, S. Ehrlich, L. Goerigk, Effect of the damping function in dispersion corrected density functional theory, J. Comput. Chem. 32 (2011) 1456.
[29] J.P. Perdew, K. Burke, M. Ernzerhof, Generalized gradient approximation made simple, Phys. Rev. Lett. 77 (1996) 3865.
[30] J. Heyd, G.E. Scuseria, M. Ernzerhof, Hybrid functionals based on a screened Coulomb potential, J. Chem. Phys. 118 (2003) 8207–8215.
[31] J. Heyd, G.E. Scuseria, M. Ernzerhof, Erratum: "Hybrid functionals based on a screened Coulomb potential", J. Chem. Phys. 124 (2006) 219906.
[32] T. Holstein, H.L. Primakoff, Field dependence of the intrinsic domain magnetization of a ferromagnet, Phys. Rev. 58 (1940) 1098.
[33] D. Stanek, O.P. Sushkov, G.S. Uhrig, Self-consistent spin-wave theory for a frustrated Heisenberg model with biquadratic exchange in the columnar phase and its application to iron pnictides, Phys. Rev. B 84 (2011) 064505.
[34] J.L. Lado, J. Fernández-Rossier, On the origin of magnetic anisotropy in two dimensional CrI_3, 2D Mater. 4 (2017) 035002.
[35] N.J. Roome, J.D. Carey, Beyond graphene: stable elemental monolayers of silicene and germanene, ACS Appl. Mater. Interfaces 6 (2014) 7743–7750.
[36] R.C. O'Handley, Modern Magnetic Materials: Principles and Applications, 1st ed., Wiley-Interscience, 1999.
[37] Y. Deng, Y. Yu, Y. Song, J. Zhang, N.Z. Wang, Z. Sun, et al., Gate-tunable room-temperature ferromagnetism in two-dimensional Fe_3GeTe_2, Nature 563 (2018) 94.